Backbone Dynamics of the Glucocorticoid Receptor DNA-Binding Domain†

Helena Berglund,‡ Helena Kovács,‡ Karin Dahlman-Wright,‡ Jan-Åke Gustafsson,§ and Torleif Härd*,‡

Center for Structural Biochemistry and Department of Medical Nutrition, Karolinska Institutet, Novum, S-141 57 Huddinge, Sweden

Received July 7, 1992; Revised Manuscript Received September 15, 1992

ABSTRACT: The extent of rapid (picosecond) backbone motions within the glucocorticoid receptor DNA-binding domain (GR DBD) has been investigated using proton-detected heteronuclear NMR spectroscopy on uniformly ^{15}N-labeled protein fragments containing the GR DBD. Sequence-specific ^{15}N resonance assignments, based on two- and three-dimensional heteronuclear NMR spectra, are reported for 65 of 69 backbone amides within the segment C440–A509 of the rat GR in a protein fragment containing a total of 82 residues (MW = 9200). Individual backbone ^{15}N spin–lattice relaxation times (T_1), rotating-frame spin–lattice relaxation times ($T_{1\rho}$), and steady-state $\{^1H\}$–^{15}N nuclear Overhauser effects (NOEs) have been measured at 11.74 T for a majority of the backbone amide nitrogens within the segment C440–N506. T_1 relaxation times and NOEs are interpreted in terms of a generalized order parameter (S^2) and an effective correlation time (τ_e) characterizing internal motions in each backbone amide using an optimized value for the correlation time for isotropic rotational motions of the protein (τ_R = 6.3 ns). Average S^2 order parameters are found to be similar ($\approx 0.86 \pm 0.07$) for various functional domains of the DBD. Qualitative inspection as well as quantitative analysis of the relaxation and NOE data suggests that the picosecond flexibility of the DBD backbone is limited and uniform over the entire protein, with the possible exception of residues S448–H451 of the first zinc domain and a few residues for which relaxation and NOE parameters were not obtained. in particular, we find no evidence for extensive rapid backbone motions within the second zinc domain. Our results therefore suggest that the second zinc domain is not disordered in the uncomplexed state of DBD, although the possibility of slowly exchanging (ordered) conformational states cannot be excluded in the present analysis.

The glucocorticoid receptor (GR)[1] belongs to the family of ligand-inducible transcription factors including the steroid hormone, thyroid hormone, vitamin D_3, and retinoic acid receptors (Evans, 1988). All members of this superfamily contain a highly conserved DNA-binding domain (DBD) consisting of about 70 residues. The DBD mediates specific binding to hormone response elements on DNA, and protein fragments containing the DBD expressed in *Escherichia coli* also bind specifically to these DNA sequences (Freedman et al., 1988; Dahlman et al., 1989). The DBD contains two zinc ions that are required for proper folding and DNA binding, in analogy with the "zinc finger" motifs found in several other transcription factors. However, the zinc-coordinating domains found in steroid/thyroid hormone receptors are structurally distinct [see Kaptein (1991) for a recent review of zinc finger structures].

The structure of the GR DBD (Figure 1) has been determined in solution using NMR spectroscopy (Härd et al., 1990a,b), and the crystal structure of the same DBD fragment in a dimeric complex with DNA has been determined using X-ray diffraction methods (Luisi et al., 1991). NMR studies of the estrogen receptor DBD (Schwabe et al., 1990) and retinoic acid receptor DBD (R. Kaptein, personal communication) reveal structures that are very similar to that of the GR DBD. The DBD consists of two subdomains that have the general composition [zinc domain–helix–extended region]. The two helices are oriented perpendicular to each other, and hydrophobic side chains of these and of the following extended regions form a protein core. The two zinc domains, which are packed against the protein body, differ structurally and functionally. The first zinc domain provides three nonspecific DNA contacts in the DBD–DNA complex, and the C-terminal residues of this domain constitute the base of the amphiphathic helix that determines sequence-specific binding by directly interacting with functional groups in the DNA major groove (Danielson et al., 1989; Mader et al., 1989; Umesuno & Evans, 1989; Luisi et al., 1991). The second zinc domain provides the entire dimerization surface for DBD–DBD interactions as well as several contacts with DNA phosphates, and it also contains amino acid residues that might be important for positive control of transcription (Schena et al., 1989).

Although there is a good agreement between NMR and X-ray structures of the GR DBD with regard to secondary structure elements, overall protein folding, and side-chain packing in the hydrophobic core, there are some remaining ambiguities regarding the conformation and conformational flexibility of the second zinc-coordinating domain. This domain (residues 476–495 of the rat GR), which protrudes out from the protein core with a zinc ion at the base, is well resolved in the crystal structure of the DBD–DNA complex, with a short loop involving residues C476–N480, a β strand encompassing D481–D485, and a (distorted) helix consisting of residues K486–N491 (Figure 1). The NMR solution

† This work was supported by a research fellowship and a grant from the Swedish Natural Sciences Research Council (T.H.) and by a postdoctoral fellowship from Karo Bio AB (H.K.), and by a grant from the Swedish Medical Research Council (No. 13x-2819).

* Author to whom correspondence should be addressed. Telephone: +46 8 608 92 30; Telefax: +46 8 608 92 90.

‡ Center for Structural Biochemistry.

§ Department of Medical Nutrition.

[1] Abbreviations: GR, glucocorticoid receptor; ER, estrogen receptor; DBD, DNA-binding domain; NOE, nuclear Overhauser enhancement; TPPI, time-proportional phase increment; CPMG, Carr–Purcell–Meiboom–Gill; DTT, dithiothreitol.

0006-2960/92/0431-12001$03.00/0

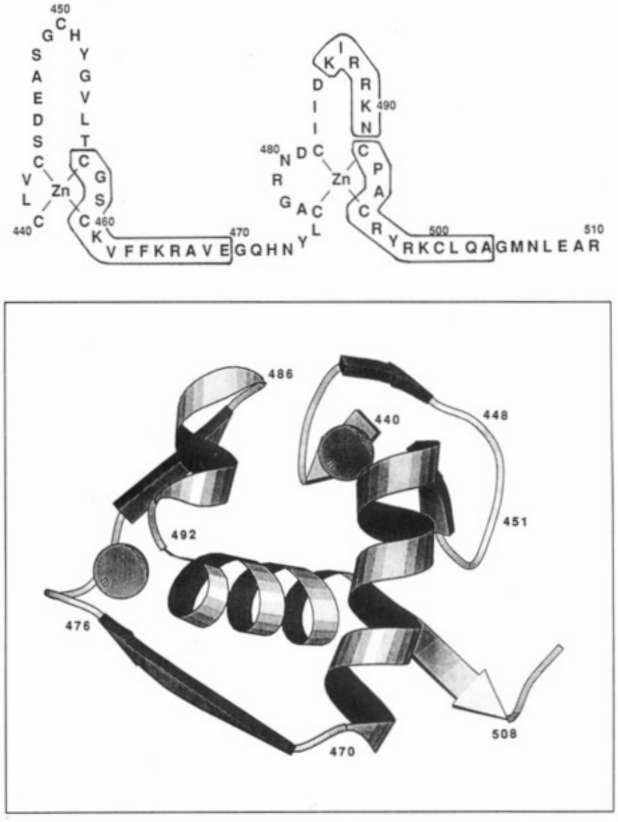

FIGURE 1: Sequence and structure of residues C440–R510 of the rat glucocorticoid receptor including the DNA-binding domain, DBD. The DBD crystal structure (Luisi et al., 1991) is drawn in a ribbon representation with the two zinc ions represented by hard spheres. The α-helical segments of this structure are boxed in the DBD sequence.

structure of this region is much less well-defined, and medium-range NOE connectivities corresponding to those secondary structure elements that are observed in the crystal have not been observed in previous studies (Härd et al., 1990a). The resolution of the second zinc domain of the estrogen receptor DBD in solution is also poor (Schwabe et al., 1990). It has been speculated that the differences between the NMR and crystal structures arise from a stabilization of secondary structure upon formation of the DNA complex (Luisi et al., 1991). According to this view, interactions between DNA and certain residues in DBD help stabilize the dimer interface, thereby causing cooperative enhancement of dimerization and DNA binding. On the other hand, large apparent disorder in loops and terminal regions resulting from too few structural (NOE) constraints is a recurring problem in structure determinations using NMR. This is because it is often impossible to determine if the lack of NOE connectivities is due to incomplete spectral analysis or to true disorder. The matter is further complicated by the fact that structural elements such as loops only result in a few NOE connectivities although the structure itself is stable and ordered.

The possible influence of dynamical processes on DBD function and possible differences between DBD in the free versus the complexed state has prompted us to initiate a series of studies of the DBD dynamics on various time scales using ^{15}N-labeled protein samples. NMR is particularly useful for studying internal motions in macromolecules because specific sites (backbone amides) can be monitored independently on time scales ranging from 10^{-11} to about 10^{-3} s in ^{15}N relaxation studies and also on much longer time scales by measuring amide proton exchange rates. Heteronuclear spin–lattice (T_1 and $T_{1\rho}$) relaxation times and nuclear Overhauser enhancements (NOEs) provide information on rapid internal motions and overall rotational motions of a protein. The rotating-frame spin–lattice relaxation time $T_{1\rho}$ (or spin–spin relaxation time T_2) and hydrogen exchange rates are also sensitive to dynamical processes that occur on longer time scales (milliseconds). Heteronuclear NMR on proteins has previously been hampered by the low natural abundance of the ^{13}C and ^{15}N nuclei as well as of the inherent insensitivity of these nuclei, compared to the ^{1}H sensitivity. However, the low natural abundance can be overcome for proteins that are overexpressed in bacteria by letting these grow in an isotopically enriched medium. The insensitivity problem was solved by the introduction of proton-detected heteronuclear NMR techniques [see Bax et al. (1989) for a review]. These developments in combination with novel 2D pulse sequences for measurement of heteronuclear relaxation rates and NOEs (Nirmala & Wagner, 1988; Kay et al., 1989; Peng et al., 1991a,b) have enabled investigations of backbone dynamics in several proteins. Studies on staphylcoccal nuclease (Kay et al., 1989), interleukin-1β (Clore et al., 1990a), the Xfin-31 zinc finger (Palmer et al., 1991), calbindin D_{9k} (Kördel et al., 1992), human ubiquitin (Schneider et al., 1992), and the *Bacillus subtilis* glucose permease IIA domain (Stone et al., 1992) show that heteronuclear relaxation and NOE measurements can be used to identify regions of the polypeptide backbone that are flexible and/or unstructured. In particular, studies on calbindin D_{9k} (Kördel et al., 1992) show that these methods allow the distinction of regions of the NMR-derived structure that are poorly defined due to a high inherent flexibility from less flexible regions that are poorly defined due to lack of structural constraints.

The present paper includes sequence-specific ^{15}N resonance assignments and an investigation of the extent of rapid backbone motions in the GR DBD. We report measurements of ^{15}N T_1 and $T_{1\rho}$ relaxation times and $\{^1$H$\}$–^{15}N NOEs for backbone amide nitrogens within the C440–N506 segment of the rat GR DBD. The data are interpreted using the formalism developed by Lipari and Szabo (1982a,b), i.e., in terms of a generalized order parameter (S^2) and an effective correlation time (τ_e) for internal motions. In summary, the flexibility of the DBD backbone seems to be limited and uniform over the entire protein, with a few possible exceptions. In particular, we find no evidence for extensive rapid backbone motions within the second zinc domain. Our results therefore strongly suggest that the second zinc domain is not disordered in the uncomplexed state of DBD and that NMR structure determinations of this domain yield poorly defined structures due to lack of structural constraints rather than to inherently high flexibility.

MATERIALS AND METHODS

Protein Purification and Sample Preparation. The fragment M(L439–Q520) (DBD-82) of the rat glucocorticoid receptor was inserted in the plasmid pT7-7 (Tabor & Richardson, 1985), kindly provided by Dr. Y. Ohara-Nemoto, and overexpressed in *E. coli*. The correct DNA insert was confirmed by sequencing. For these studies cells were grown in a minimal medium with $^{15}NH_4Cl$ (99.8% ^{15}N; Larodan AB, Sweden) as the only nitrogen source. Cell lysates were fractioned with ammonium sulfate, and the protein was purified by elution from a CM-Sepharose column with a linear 125–400 mM NaCl salt gradient in a 20 mM phosphate buffer at pH 7.6, with 1 mM DTT. In cases where this step did not yield a pure sample, an additional elution from a Mono S FPLC column (Pharmacia) was performed with a 50–500

mM NaCl salt gradient in 20 mM phosphate and 1 mM DTT at pH 7.6. The protein was completely pure as judged from SDS gel electrophoresis. NMR samples in 250 mM NaCl, 20 mM phosphate, and 2 mM DTT at pH 7.6 were concentrated using Centricon filters to a final concentration of approximately 0.9 mM. The NMR tube with sample was repeatedly flushed with nitrogen followed by equilibration to minimize the amount of dissolved oxygen. NMR studies of steroid/hormone receptor DBDs are known to be difficult due to protein instability and aggregation. However, our procedures have yielded NMR samples that have not shown significant precipitation during the time (several months) that data were collected.

NMR Spectroscopy. All experiments were performed on a Varian Unity 500 NMR spectrometer at a magnetic field of 11.74 T using an inverse probe. Proton chemical shifts at 299 K are referenced to H_2O at 4.75 ppm, and ^{15}N chemical shifts at 299 K are referenced to external [^{15}N]benzamide at 105.4 ppm (Levy & Lichter, 1979).

Sequential assignments of ^{15}N resonances in the GR DBD are based on several types of two- and three-dimensional ^1H–^{15}N correlation spectra including HMQC (Müller, 1979; Bax et al., 1983), HMQC-NOESY and HMQC-TOCSY (Gronenborn et al., 1989a), HSQC-NOESY (Bax et al., 1990), and 3D NOESY-HMQC and 3D TOCSY-HMQC (Marion et al., 1989a). Two-dimensional heteronuclear spectra used for ^{15}N assignments were recorded in hypercomplex mode (States et al., 1982) using ^{15}N and ^1H spectral widths of 3000 and 6000 Hz, respectively, with 128–256 t_1 increments, 64–256 transients/increment, and 1024 complex data points/transient. The water resonance was in all cases supressed by (weak) presaturation during relaxation and evolution delays. Data processing (using FELIX from Hare Research) involved apodization with shifted Gaussian functions and sine/cosine bell functions in the t_2 and t_1 domains, respectively, zero filling to 2048 × 2048 real data points, and polynomial base-line correction. Recorded free induction decays were subjected to a high-pass filter before Fourier transformation to remove the major part of the residual water signal (Marion et al., 1989b).

Three-dimensional heteronuclear NOESY-HMQC and TOCSY-HMQC spectra were recorded at 289 and 299 K (total of four 3D spectra) in "super-hypercomplex" mode using 2 × 160 t_1 increments, 2 × 32 t_2 increments (^{15}N domain), 512 complex data points in the aquisition domain, and 8 and 16 transients/increment in the NOESY-HMQC and TOCSY-HMQC spectra, respectively. The mixing time was 150 ms in NOESY-HMQC spectra, and the clean-TOCSY spin lock (Griesinger et al., 1988) mixing time was 50 ms in TOCSY-HMQC spectra. Spectral widths were 6000 Hz in the two ^1H domains and 2000 Hz in the ^{15}N domain. The spectra were processed using Varian software (VNMR 4.1) on a Sun Sparc 330 work station. Processed matrices contained 1024 × 64 × 1024 real data points. Base-line correction was applied in the F_3 (acquisition) domain prior to Fourier transformation of the t_1 and t_2 domains. Aquisition domain data were apodized using Gaussian functions, and cosine bell apodization was applied to the t_1 and t_2 domains prior to Fourier transformation.

^{15}N relaxation parameters and heteronuclear NOEs were measured at 299 K using somewhat modified versions of the double-INEPT (Bodenhausen & Ruben, 1980) pulse sequences initially described by Kay et al. (1989). The relaxation and NOE experiments were all carried out in TPPI mode (Marion & Wüthrich, 1983) with an ^{15}N spectral width of 3000 Hz (^{15}N transmitter at 122.4 ppm), a ^1H spectral width of 6000 Hz (transmitter at H_2O resonance), using values of the Δ and τ refocusing delays (Kay et al., 1989) of 1.8 and 2.1 ms, respectively, and using WALTZ decoupling of ^{15}N during the acquisition period. The water signal was suppressed by presaturation during relaxation and evolution delays, except in the NOE experiment where water suppression was achieved using a short (2-ms) spin lock pulse immediately preceding the t_1 evolution period. Spectra were recorded with 256 t_1 increments, 32 (T_1 and $T_{1\rho}$ experiments) or 256 (NOE experiment) transients/increment, and 1024 complex data points/transient.

The T_1 inversion–recovery experiment was recorded as described by Kay et al. (1989), with the exception that protons were decoupled using a WALTZ-16 decoupling sequence during the T_1 recovery delays. The relaxation delay between successive transients was 3.0 s. Seven spectra were recorded interleaved (16 transients/block) with T_1 recovery periods of 12, 94, 189, 342, 496, 992, and 2999 ms. The full T_1 experiment was performed three times corresponding to a total data collection time of about 8 days.

^{15}N $T_{1\rho}$ relaxation times were measured according to Peng et al. (1991b). A spin lock sequence consisting of consecutive 180° pulses at a power corresponding to an effective spin lock field of 3700 Hz was applied during the $T_{1\rho}$ recovery delays. The relaxation delay between successive transients was 2.8 s. Seven spectra were recorded interleaved (16 transients/block) with $T_{1\rho}$ recovery periods of 8.4, 34, 55, 89, 148, 279, and 498 ms. The $T_{1\rho}$ experiment was performed once (within 2.5 days).

{^1H}–^{15}N NOEs were measured according to Kay et al. (1989). Spectra recorded with and without the heteronuclear NOE were recorded interleaved as in the relaxation measurements. Transients recorded with NOE were preceded by 120° ^1H saturation pulses with a spacing of 20 ms applied during 3 s, with an initial relaxation delay of 1.8 s preceding this pulse train. Transients recorded without NOE were preceded with a corresponding 4.8-s relaxation delay. The pulse sequence was tested on a sample of glucose-2-^{13}C, for which an {^1H}–^{13}C NOE corresponding to $I/I_0 = 2.98$ was measured. The NOE experiment was performed three times with a total data collection time of about 15 days.

Relaxation and NOE data were processed using VNMR 3.2A and 4.1 software from Varian and FELIX from Hare Research. Time domain data were apodized using line broadening or shifted Gaussian functions for the t_2 (acquisition) domain and line broadening, cosine bell, or shifted sine bell functions for the t_1 domain. Zero filling was used in both time domains to obtain typical sizes of 1024 × 2048 real data points in Fourier transformed spectra. Polynomial (FELIX) or spline function (VNMR) base-line corrections were in all cases applied in the F_2 frequency domain prior to Fourier transformation of the (F_2, t_1) interferogram.

Determination of Relaxation Parameters and NOEs. T_1 relaxation times were determined from peak heights measured in processed two-dimensional ^1H–^{15}N correlation spectra. Peak heights of nonoverlapping cross-peaks were measured in spectra processed with cosine bell apodization functions, whereas peak heights of (slightly) overlapping cross-peaks were measured in spectra processed with shifted sine bell apodization functions. Uncertainties due to noise (σ_{noise}) in measured peak heights were in each case estimated from the base-line noise level. Typical values of σ_{noise} were ≈2–4% of the peak height (signal/noise ≈25–40) of the first spectrum in the T_1 experiment. Some resonances with a lower signal/noise ratio were excluded from further analysis. Data analysis was carried out using the MATLAB software package

(MathWorks, Inc.). T_1 (and $T_{1\rho}$) relaxation times were obtained by fitting experimental data to the functional form $A + B\exp(t/T_i)$ ($i = T_1, T_{1\rho}$) using nonlinear least-squares curve fitting based on the Nelder–Meade simplex algorithm. Fitted decays were single-exponential within experimental uncertainties. The determined T_1 relaxation times shown in Figure 4 represent averages (with estimated standard deviations) of three completely independent T_1 determinations carried out for each amide ^{15}N.

Heteronuclear NOEs (I/I_0) were determined in an analogous manner from peak heights in spectra recorded with (I) and without (I_0) the heteronuclear NOE. Signal to noise ratios for resonances in spectra recorded without NOE were approximately equal to, or better than, corresponding intensities in the first spectrum of the T_1 experiments. Reported NOEs (Figure 4) are averages with estimated standard deviations calculated from three independent determinations.

$T_{1\rho}$ relaxation times were determined from a single experiment, in which the intensities at each increment were obtained from cross-peak volume integrations in spectra processed with Gaussian apodization functions. Uncertainties were estimated from integrations of representative regions of the noise floor. Curve fitting was carried out as with the T_1 data. The results are shown in Figure 4, where the error bars in this case represent estimated standard deviations derived from the covariance matrix for parameters obtained from the least-squares optimization (Press et al., 1986), rather than from several independent determinations.

Theoretical Considerations. The T_1 (spin–lattice) relaxation and the {^{1}H}–^{15}N NOE of a peptide amide ^{15}N are dominated by dipolar interactions with the directly bonded proton and by the chemical shift anisotropy (Abragam, 1961; Kay et al., 1989). The relaxation parameters and the NOE are functions of the spectral density function, $J(\omega)$, which is the Fourier transform of the orientational correlation function for motions of a unit vector colinear with the ^{15}N–^{1}H bond. Following Kay et al. (1989) we write the relaxation parameters and the steady-state NOE as

$$1/T_1 = d^2[J(\omega_A - \omega_X) + 3J(\omega_X) + 6J(\omega_A + \omega_X)] + c^2J(\omega_X) \quad (1)$$

$$\mathrm{NOE} = 1 + T_1(\gamma_A/\gamma_X)d^2[6J(\omega_A + \omega_X) - J(\omega_A - \omega_X)] \quad (2)$$

with $d^2 = (1/10)\gamma_A^2\gamma_X^2(h^2/4\pi^2)\langle 1/r_{AX}^3\rangle^2$ and $c^2 = (2/15)\gamma_X^2H_0^2(\sigma_\parallel - \sigma_\perp)$, and where A = ^{1}H, X = ^{15}N, γ_i and ω_i are the gyromagnetic ratio and Larmor frequency of spin i, respectively, r_{AX} is the internuclear ^{1}H–^{15}N distance (1.02 Å) (Keiter, 1986), H_0 is the magnetic field strength, and $\sigma_\parallel - \sigma_\perp$ (=–160 ppm) is the difference between the parallel and perpendicular components of the ^{15}N chemical shift tensor (Hiyama et al., 1988).

T_2 (spin–spin) relaxation times of ^{15}N nuclei in amides that are not involved in dynamic equilibria (chemical exchange) are also dominated by the dipolar and chemical shift anisotropy relaxation mechanisms. Unfortunately, when exchanging states are involved, this parameter becomes "contaminated" by an exchange term that is difficult to access experimentally [see, for instance, Clore et al. (1990a)]. In addition, there has been a recent discussion in the literature regarding the correct method for measuring T_2 relaxation times (Kay et al., 1989; Peng et al., 1991b). Peng et al. argues that T_2 measurements using a CPMG spin-echo pulse train result in measured T_2 values that are artificially shortened due to contributions from rapid relaxation of antiphase coherences that develop during the refocusing delays of the CPMG pulse sequence and that this problem is avoided if one instead measures the spin–lattice relaxation time in the rotating frame ($T_{1\rho}$), by applying an on-resonance spin lock instead of the CPMG pulse train used by some other groups, e.g., Kay et al. (1989) and Palmer et al. (1991).

In this work we measure spin–lattice relaxation in the rotating frame ($T_{1\rho}$) by applying a 3.7-kHz on-resonance spin lock during the ^{15}N recovery delay, following Peng et al. (1991b). In the quantitative analysis of the overall protein reorientation motions, described in more detail below, we only use measured $T_{1\rho}$ values for ^{15}N resonances that are located within ±200 Hz of the transmitter, for which the error in $T_{1\rho}$ due to frequency offset can be expected to be <2%.

If a weak on-resonance spin lock is used, and if the spectral density functions are assumed to be Lorentzians, then $T_{1\rho}$ relaxation is theoretically indistinguishable from T_2 relaxation, with the exception that a $J(0)$ spectral density term (Kay et al., 1989) is replaced by a $J(\omega_e)$ spectral density term, where ω_e is the frequency of the spin lock field (Peng et al., 1991a). In analogy with eqs 1 and 2 above we write

$$1/T_{1\rho} = (1/2)d^2[4J(\omega_e) + J(\omega_A - \omega_X) + 3J(\omega_X) + 6J(\omega_A) + 6J(\omega_A + \omega_X)] + (1/6)c^2[3J(\omega_X) + 4J(\omega_e)] \quad (3)$$

The spectral density $J(\omega)$ for a macromolecule in solution depends on the overall rotational motion of the protein as well as on internal motions. The internal motions might be complex, involving several processes on various time scales (McCammon & Harvey, 1987; Clore et al., 1990a,b). It is desirable to approximate the spectral density function using a small number of physically meaningful parameters that can be determined experimentally. In the formalism of Lipari and Szabo internal motions are characterized by two parameters: a generalized order parameter, S^2, and an effective internal correlation time, τ_e (Lipari & Szabo, 1982a,b). The generalized order parameter is a measure of the spatial restriction of the ^{15}N–^{1}H bond vector. A value of $S^2 = 1$ would be obtained for a completely rigid system, whereas $S^2 = 0$ indicates completely unrestricted internal motions. The τ_e parameter is an effective correlation time for internal motions, and it depends on both the rate and amplitude of these motions. If the overall rotational motion of the protein is isotropic with a rotational correlation time τ_R, then the spectral density can be written (Lipari & Szabo, 1982a,b)

$$J(\omega_i) = S^2\tau_R/[1 + (\omega_i\tau_R)^2] + (1 - S^2)\tau/[1 + (\omega_i\tau)^2] \quad (4)$$

where $\tau^{-1} = \tau_e^{-1} + \tau_R^{-1}$.

In cases where the overall rotational motion is anisotropic one can approximate the spectral density as (Lipari & Szabo, 1982a)

$$J(\omega_i) = S^2\{A\tau_1/[1 + (\omega_i\tau_1)^2] + (1 - A)\tau_2/[1 + (\omega_i\tau_2)^2]\} + (1 - S^2)\{A\tau_{1e}/[1 + (\omega_i\tau_{1e})^2] + (1 - A)\tau_{2e}/[1 + (\omega_i\tau_{2e})^2]\} \quad (5)$$

where $1/\tau_{1e} = 1/\tau_1 + 1/\tau_e$ and $1/\tau_{2e} = 1/\tau_2 + 1/\tau_e$. Here, the two correlation times τ_1 and τ_2 and the mixing parameter A describe anisotropic overall rotational motion. The case $A = 0.5$ corresponds to $\tau_1 = \tau_2$, i.e., isotropic motion.

Analysis of Relaxation and NOE Data. In order to quantify relaxation and NOE data in terms of parameters for internal and overall motions we first used T_1, $T_{1\rho}$, and NOE data for a selected set of residues (see below) to obtain a value for the overall rotational correlation time, τ_R. This was done by

minimizing the function

$$\sum\chi_i^2 = \sum(T_{1,\mathrm{exp},i} - T_{1,\mathrm{calc},i})^2/\sigma_{\mathrm{T1},i}^2 + (T_{1\rho,\mathrm{exp},i} - T_{1\rho,\mathrm{calc},i})^2/\sigma_{\mathrm{T1}\rho,i}^2 + (\mathrm{NOE}_{\mathrm{exp},i} - \mathrm{NOE}_{\mathrm{calc},i})^2/\sigma_{\mathrm{NOE},i}^2 \quad (6)$$

where the sum extends over all residues i for which the minimization is carried out and where $T_{1,\mathrm{exp}}$, $T_{1\rho,\mathrm{exp}}$, and $\mathrm{NOE}_{\mathrm{exp}}$ are the experimentally determined values for T_1, $T_{1\rho}$, and the NOE for each residue, respectively, σ_{T1}, $\sigma_{\mathrm{T1}\rho}$, and σ_{NOE} are the corresponding estimated standard deviations, and $T_{1,\mathrm{calc}}$, $T_{1\rho,\mathrm{calc}}$, and $\mathrm{NOE}_{\mathrm{calc}}$ are calculated from eqs 1–4. The minimization corresponds to a global fit of τ_R, because the number of experimental observations in eq 6 exceeds the number of optimized parameters. Errors in the calculation of τ_R, and S^2 and τ_e for each residue, were estimated using Monte Carlo simulations (Press et al., 1986): "synthetic" sets of T_1, $T_{1\rho}$, and NOE data were generated for each residue by drawing random numbers with means corresponding to $T_{1,\mathrm{exp}}$, $T_{1\rho,\mathrm{exp}}$, and $\mathrm{NOE}_{\mathrm{exp}}$ and using σ_{T1}^2, $\sigma_{\mathrm{T1}\rho}^2$, and σ_{NOE}^2 as variances of normal distribution functions, respectively. The minimization was carried out for each set of synthetic data, and standard deviations of the optimized parameters were calculated. These errors correspond to "real" errors as long as the shapes of the distribution functions for repeated experimental determinations of the relaxation and NOE parameters are similar to the probability distributions for observations of the "true" relaxation and NOE parameters (Press et al., 1986). The possibility of anisotropic overall motions was also investigated using eq 5 in place of eq 4 (optimizing τ_1, τ_2, and A).

The optimized value of the overall rotational correlation time, τ_R, was then used in "local" optimizations of S^2 and τ_e for all residues from the corresponding T_1 and NOE data ($T_{1\rho}$ data were not used here). This calculation was carried out in an analogous manner, and Monte Carlo simulations were used to estimate uncertainties in the determined parameters.

RESULTS AND DISCUSSION

Assignment of Amide ^{15}N Resonances. Sequential assignments of ^{15}N resonances in two- and three-dimensional heteronuclear spectra were carried following the general methods outlined by Gronenborn et al. (1989b) and Marion et al. (1989a). The assignments are based on the previously assigned ^1H spectrum of GR DBD (Härd et al., 1990a). A sensitivity-enhanced ^1H–^{15}N HMQC spectrum of DBD-82 (not shown) contains about 70 unique backbone amide cross-peaks. A majority of the 10 missing resonances belongs to the unstructured C-terminal tail of the DBD and are therefore not visible due to rapid exchange with the solvent at pH 7.6. About 15 ^{15}N resonances could be assigned on the basis of the unique ^1H chemical shift of the corresponding amide cross-peak. These assignments were taken as starting points for sequential assignments using characteristic d_{NN} NOE connectivities (Härd et al., 1990a), which were relatively easy to locate in 2D HSQC-NOESY spectra, providing about 25 additional assignments. The amide ^{15}N resonances of a few spin systems identified in HMQC-TOCSY (e.g., T456) could be assigned on the basis of chemical shifts of $C^\alpha H$ and side-chain protons. The remainder of the ^{15}N assignments reported here were obtained through almost complete assignments of 3D NOESY-HMQC spectra at 289 and 299 K (Figure 2), using the corresponding 3D TOCSY-HMQC spectra as an aid when distinguishing between intraresidue NOEs and sequential NOE connectivities. The 3D NOESY-HMQC spectra contain almost all of the previously identified amide NOE connectivities, which were used in the previous structure determination of the GR DBD (Härd, 1990b), as well as several novel NOE connectivities, which are overlapped in homonuclear NOESY spectra. A total of 65 out of 69 backbone amide ^{15}N resonances within the segment C440–A509 in DBD-82 were sequentially assigned, and the corresponding ^{15}N and $C^\alpha H$ chemical shifts are listed in Table I. ^{15}N assignments are missing for C450, H451, N473, and K490. The amide proton resonances of C450 and H451 cannot be located in homonuclear spectra of DBD-82, and these amide protons are probably in rapid exchange with the solvent. The $C^\alpha H$ resonance of N473 is located very close to the H_2O resonance at both 289 and 299 K, and cross-peaks involving this resonance might be weak as a result of the water presaturation, possibly in combination with exchange broadening. The K490 amide proton is not firmly assigned in homonuclear spectra. ^{15}N resonance assignments are also missing for the C-terminal segment R510–Q520, because this segment is largely unstructured in recombinant DBD fragments (Härd et al., 1990a,b; Luisi et al., 1991). A few ^{15}N resonance assignments are less firm due to lack of sequential NOE connectivities and these are indicated in Table I. The present assignments of NH protons in the DBD-82 fragment differ only slightly from previously reported assignments in a longer GR DBD fragment (Härd et al., 1990a), with two exceptions: The NH proton of S448 is reassigned and an assignment of the G449 NH is added.

Determination of ^{15}N Relaxation Times and Heteronuclear NOEs. Some typical T_1 and $T_{1\rho}$ relaxation decays and the corresponding least-squares fits to monoexponential decays are shown in Figure 3. All experimentally determined ^{15}N T_1 relaxation times, ^{15}N $T_{1\rho}$ relaxation times, and steady-state $\{^1H\}$–^{15}N NOEs are shown in Figure 4. NOEs were determined for 61 of 68 amide nitrogens within the segment C440–E508. NOEs are not reported for four residues for which assignments are missing, and not for Q471, which is overlapped, or N491, for which the intensity was too low to allow reliable measurements. The cross-peaks of Q471 and V462 overlap rather severely at 299 K. Relaxation times and the NOE for the corresponding cross-peak are assigned to V462, for which the cross-peak has a higher intensity under nonoverlapping conditions (289 K). The A494 amide cross-peak is not overlapped in any of the experiments recorded with water presaturation. In the NOE experiment, however, it is overlapped by a cross-peak with a negative NOE, probably originating from a residue in the disordered (and flexible) C-terminal segment. The NOE spectrum contains a small number of such nonassigned cross-peaks with negative NOEs (not shown), but A494 is the only assigned cross-peak that overlaps with one of these. T_1 and $T_{1\rho}$ relaxation times are reported for 54 and 51 amide nitrogens, respectively. Relaxation times are not reported for some residues due to poor signal/noise ratios of the corresponding cross-peaks.

Most of the measured $\{^1H\}$–^{15}N NOEs fall within a narrow range around the mean (0.73 ± 0.04). Only three measured NOEs within C440–E508 are lower than 0.65. The corresponding residues are G449, Y474, and E508 for which the NOEs 0.62 ± 0.03, 0.63 ± 0.08, and 0.58 ± 0.03 were measured.

The average T_1 relaxation time is 0.46 ± 0.03 s. Four residues exhibit T_1 values that differ from the average by more than two standard deviations. These are G478 and I483, for which T_1 was measured to 0.53 ± 0.02 and 0.54 ± 0.02 s, respectively, and G453 and R489, for which T_1 is 0.36 ± 0.05 and 0.39 ± 0.01 s, respectively.

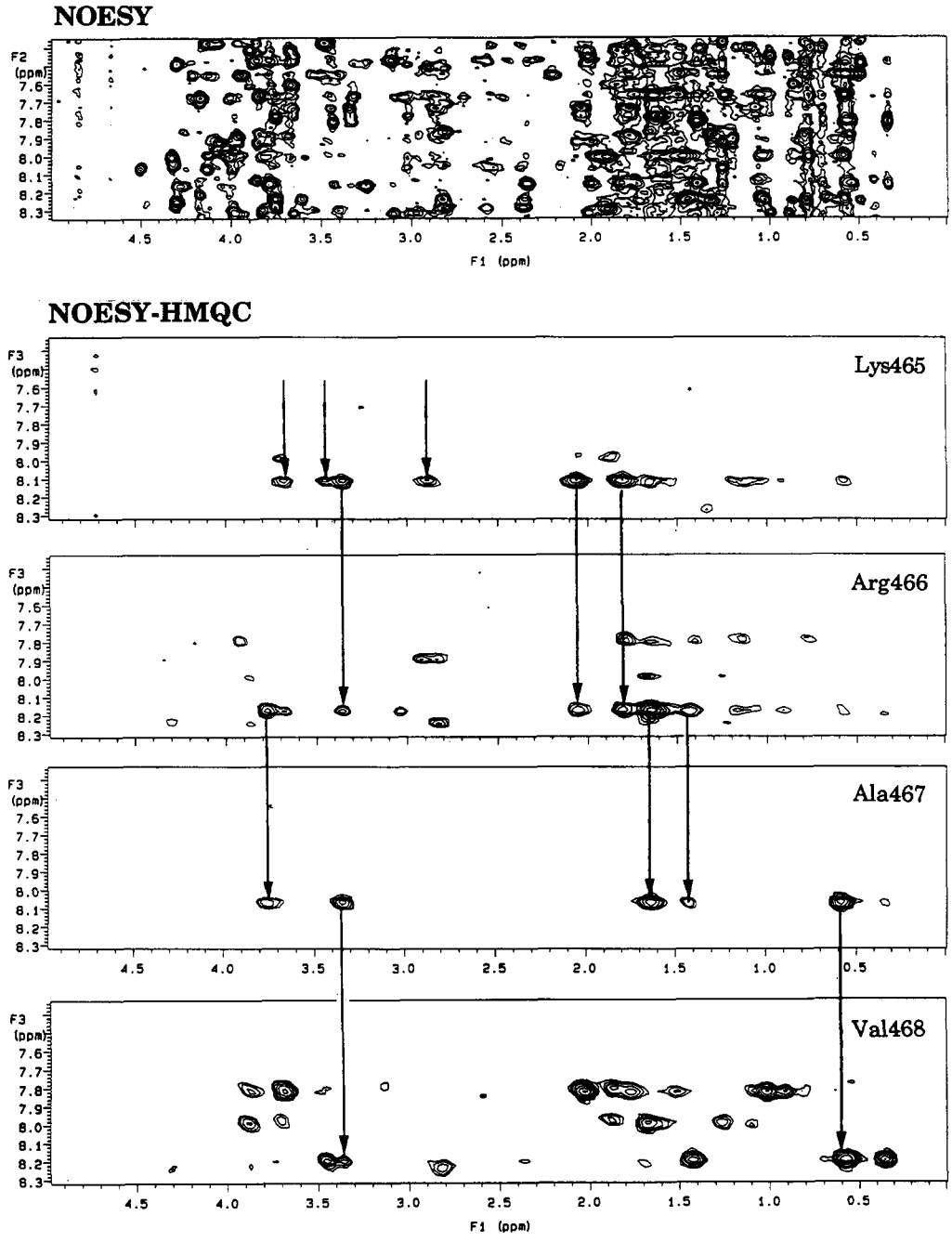

FIGURE 2: Sequential assignment of amide ^{15}N resonances in a 3D NOESY-HMQC spectrum of GR DBD at 289 K, pH 7.6. The four (F_1, F_3) planes of the spectrum shown here correspond to the amide ^{15}N resonances (in the F_2 dimension) of the four residues in the segment K465–V468. Arrows represent sequential $d_{\alpha N}$ and $d_{\beta N}$ NOE connectivities. The corresponding region of a homonuclear NOESY spectrum is shown as a reference.

The average measured $T_{1\rho}$ is 0.13 ± 0.02 s. Only one of the residues for which $T_{1\rho}$ could be determined (S444) has a $T_{1\rho}$ that is more than two standard deviations shorter than the average (0.078 ● 0.006 s).

For one unassigned ^{15}N resonance, possibly belonging to the amide of the C-terminal Q520, T_1 = 0.90 ± 0.03 s, $T_{1\rho}$ > 1 s, and the NOE = −2.37 ± 0.1, indicating a very high mobility of the amide of this residue (see below).

Comment Regarding NOE Measurements on Exchanging Amide Protons. It has been pointed out that when the T_1 of water is sufficiently long compared to the relaxation delay used in the NOE experiment, then the measured NOEs for exchanging amide protons may be artificially decreased due to incomplete equilibration of the amide ^{15}N and ^1H during the relaxation delay of the experiment recorded without proton saturation (Smith et al., 1987; Kay et al., 1989). The intrinsic exchange rate of a peptide amide proton at the present conditions (299 K, pH 7.6) approaches 25 s^{-1} (Wüthrich & Wagner, 1979). Detailed exchange data have not yet been obtained for the GR DBD, although some amide protons with exchange rates in the order of $days^{-1}$ have been identified (Härd et al., 1990a). We have measured a water T_1 = 2.5 ± 0.04 s (using a detuned probe) under the present conditions. For a rapidly exchanging proton and an effective relaxation delay of 5 s, the steady-state magnetization of the proton at the end of the relaxation delay will be about 85% of the equilibrium magnetization. The steady-state ^{15}N magnetization is $(0.85 + 0.15\text{NOE})I_{\text{equil.}}$, where $I_{\text{equil.}}$ is the equilibrium magnetization. "True" NOEs of 0.60 and 0.70 would, in this case, correspond to measured NOEs of 0.64 and 0.73, respectively. Note, however, that this is the worst-case scenario and that most amide protons in DBD are likely to have

Table I: Backbone Amide ^{15}N Resonance Assignments of GR DBD at 299 K, pH 7.6[a]

residue	^{15}N	N^1H	residue	^{15}N	N^1H
C440	124.4	9.37	L475[b]	129.5	8.73
L441	135.2	8.76	C476	132.6	9.00
V442	124.4	9.07	A477	136.0	9.45
C443	120.6	8.50	G478	118.3	9.84
S444	115.2	7.81	R479	129.5	8.79
D445	122.8	8.74	N480	121.1	9.24
E446	124.9	8.90	D481	119.2	8.16
A447	129.5	8.62	C482	126.7	8.39
S448	117.4	9.18	I483	125.5	8.28
G449	111.8	7.71	I484	130.6	8.51
C450			D485	127.7	6.58
H451			K486	121.4	8.43
Y452	121.7	8.92	I487	117.5	7.50
G453	104.0	8.24	R488	121.4	8.55
V454	121.5	7.59	R489	121.1	8.14
L455	130.9	8.30	K490		
T456	119.2	8.59	N491[b]	124.8	8.00
C457	120.2	9.27	C492	118.7	6.75
G458	119.0	7.95	P493		
S459	119.7	8.08	A494	122.8	7.94
C460	128.3	9.60	C495	125.7	9.71
K461	122.3	7.77	R496	124.7	8.48
V462	119.5	7.54	Y497	123.7	9.31
F463	123.4	8.41	R498	121.6	8.39
F464	123.6	8.70	K499	122.5	8.13
K465	120.4	7.83	C500	122.0	8.47
R466	118.2	7.92	L501	121.6	7.97
A467	125.5	7.82	Q502	124.7	8.85
V468	119.2	7.91	A503	122.1	8.05
E469	122.5	8.24	G504	104.5	7.48
G470	107.4	7.60	M505	123.0	7.65
Q471	121.5	7.58	N506	120.7	8.55
H472	120.0	7.67	L507	127.8	9.06
N473			E508	122.5	8.44
			A509[b]	126.8	8.09
Y474	124.8	8.05			

[a] Chemical shifts are given in ppm, using references as described in Materials and Methods. Chemical shifts of corresponding amide protons are also listed. [b] Less firm assignments.

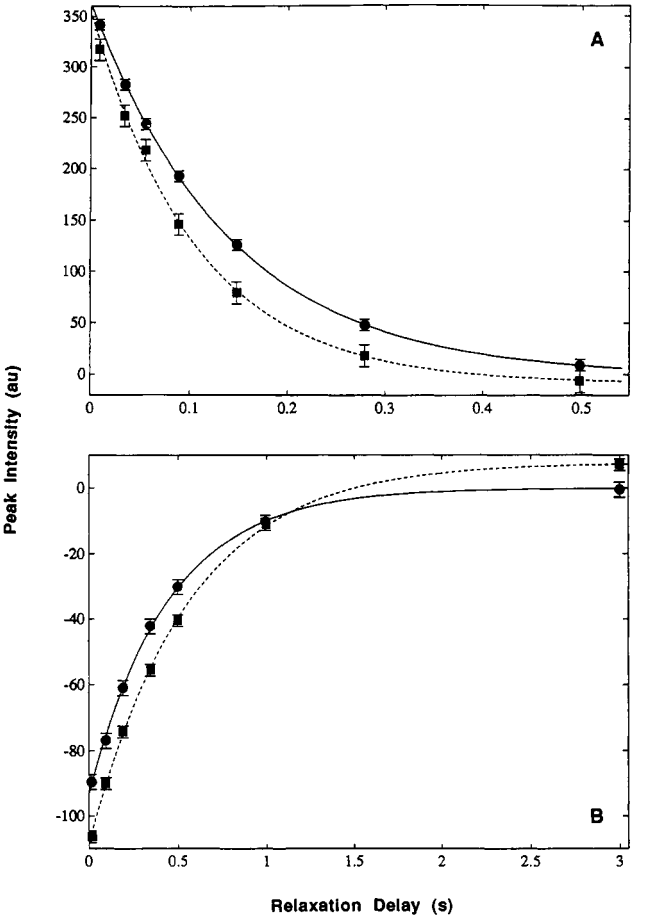

FIGURE 3: Typical relaxation decay curves obtained in the T_1 and $T_{1\rho}$ measurements on ^{15}N-labeled GR DBD at 299 K, pH 7.6 (A) ^{15}N $T_{1\rho}$ relaxation in residues V468 (●) and T456 (■). (B) ^{15}N T_1 relaxation in residues I484 (●) and L441 (■). Error bars represent estimated standard deviations. Solid and broken lines represent the results of least-squares fits to monoexponential decays, as described in the text.

exchange rates that are much longer than the intrinsic rate. In the case of the present study, possible small errors in some NOE measurements due to incomplete relaxation of water are within the order of other experimental uncertainties and would not affect any of the conclusions regarding internal flexibility.

Characterization of Overall Rotational Motion. The correlation time for overall rotational motion, τ_R, was optimized using measured T_1, $T_{1\rho}$, and NOE values for a set of 17 selected residues: K461–E469 and R496–A503. These residues were selected because the corresponding amide protons can be expected to be hydrogen-bonded within α-helical segments that are well resolved in both the crystal and solution structures of GR DBD (Luisi et al., 1991; Härd et al., 1990b). Thus, they are not likely to be involved in any slow conformational exchange equilibria that might affect $T_{1\rho}$ through $J(\omega_e)$. All ^{15}N resonances of these residues are also located within ±200 Hz of the transmitter frequency in the $T_{1\rho}$ experiment and are therefore not expected to contain significant errors due to incomplete spin locking, as discussed above. The optimization was carried out as described in the Materials and Methods section, yielding $\tau_R = 6.3 \pm 0.1$ ns. Values for the (local) parameters characterizing internal motions obtained from this global analysis are given in Table II.

The possibility of anisotropic overall rotational motion (eq 5) was also investigated, yielding $\tau_1 = 7.1 \pm 0.8$ ns, $\tau_2 = 5.78 \pm 0.9$ ns, and $A = 0.46 \pm 0.05$. In this case, τ_1 and τ_2 are not very different and the global minimum of eq 6 is rather broad considering the larger uncertainties in τ_1 and τ_2, compared to the optimization of τ_R in the isotropic model. The optimized value of the mixing parameter, A, is also close to 0.5, which is the special case of the anisotropic motion model that corresponds to isotropic motion. These results suggest that an anisotropic model of the overall rotation is not supported by the data and that further characterization of internal motion of all amides can be carried out assuming isotropic overall motion, characterized by a single correlation time.

The value of τ_R obtained above is somewhat larger than expected considering the size of the molecule (82 residues, MW = 9200) and also in view of results from similar evaluations of τ_R reported in the literature. The correlation time for isotropic rotational motion of a hydrated spherical protein with a molecular weight of 9200 can be estimated to ≈3.8 ns using the Stokes–Einstein relation (Cantor & Schimmel, 1980). The residues C440–R510 of the GR DBD form an oblate shaped body with an approximate axial ratio of 1.75 (Härd et al., 1990b; Luisi et al., 1991). Due to increased frictional forces, such a protein can be expected to have a rotational correlation time that exceeds that of a spherical protein with the corresponding volume by about 7% (Cantor & Schimmel, 1980), resulting in an (effective) τ_R of about 4.1 ns. (Note, however that the difference between the two correlation times describing the rotational motion of such a body is less than 25%.) The values $\tau_R = 4.1$ ns for ubiquitin

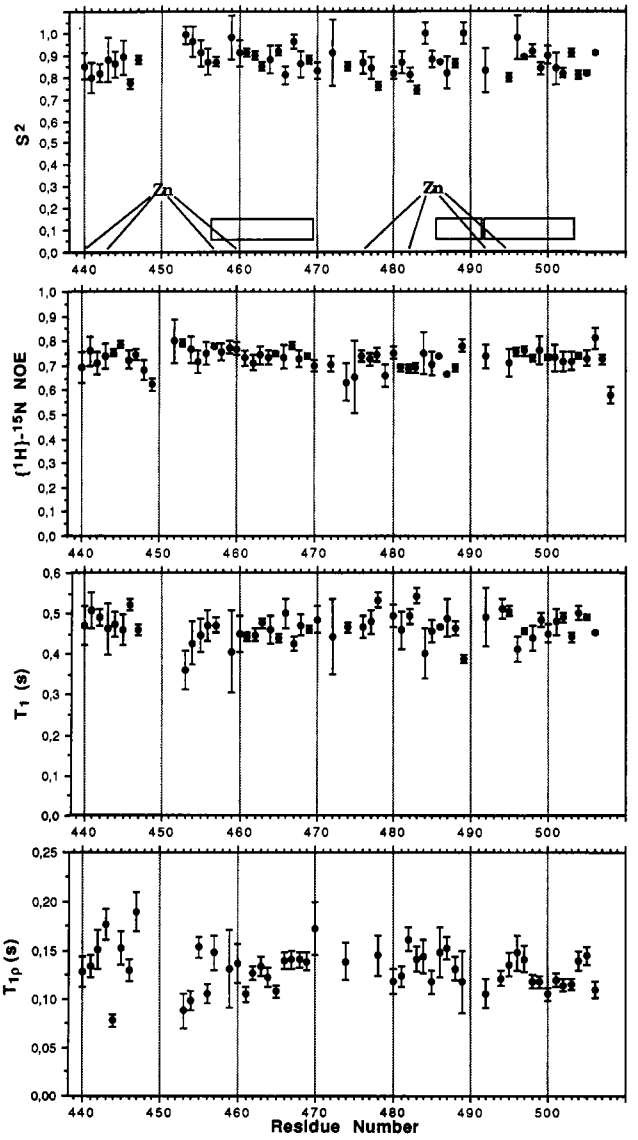

FIGURE 4: Summary of measured ^{15}N T_1 relaxation times, ^{15}N $T_{1\rho}$ relaxation times, steady-state heteronuclear $\{^1H\}$–^{15}N NOEs, and optimized S^2 order parameters for internal protein motions. Error bars represent estimated standard deviations in measured and calculated values. Zinc ion coordination and α-helical domains are indicated.

(76 residues) at 303 K (Schneider et al., 1992) and τ_R = 4.25 ns for calbindin D_{9k} (75 residues) at 300 K (Kördel et al., 1992) are reported in ^{15}N relaxation studies of these proteins, where τ_R was optimized in a similar way. A plausible explanation of the slow rotational motions of DBD-82 is that the segment K511–Q520, which appears to be largely unstructured (Härd et al., 1990b; Luisi et al., 1991), causes some additional friction. It is also possible that some of the dimerization interactions that contribute strongly to the cooperative binding of DBD to DNA (Härd et al., 1990c; Luisi et al., 1991) also take place in the uncomplexed state at the concentration used for NMR studies, although there is no additional support, such as intermolecular NOEs, for this possibility.

Relative Sensitivity of Measured Parameters to Backbone Flexibility. Modeling of eqs 1–3 shows that the relative sensitivities of the T_1 and $T_{1\rho}$ ^{15}N relaxation times and the $\{^1H\}$–^{15}N NOE to internal motions are different for motions of various kinds occurring on different time scales. Rapid (picosecond) backbone motions in a protein with an overall rotational correlation time of τ_R = 6.3 ns are primarily manifested in a lowering of the NOE and an increase of T_1. For instance, a hypothetical completely "stiff" backbone would result in NOEs approaching ≈0.78 with $T_1 \approx 0.4$ s. Structured regions with moderate flexibility ($S^2 \approx 0.7$–0.9 and $\tau_e \approx$ 10–

Table II: Optimized Parameters for Internal Motions in DBD[a]

residue	S^2	τ_e (ps)
C440	0.85 ± 0.06	
L441	0.80 ± 0.07	
V442	0.82 ± 0.04	33 ± 21
C443	0.88 ± 0.10	
S444	0.86 ± 0.06	
D445	0.89 ± 0.08	
E446	0.77 ± 0.02	20 ± 12
A447	0.88 ± 0.02	27 ± 18
S448		
G449		
C450		
H451		
Y452		
G453	0.99 ± 0.04	
V454	0.96 ± 0.07	
L455	0.91 ± 0.06	
T456	0.87 ± 0.06	
C457	0.87 ± 0.02	≈0 ± 5
G458		
S459	0.98 ± 0.10	
C460	0.91 ± 0.06	
K461	0.91 ± 0.02 (0.93 ± 0.02)	
V462	0.90 ± 0.02 (0.89 ± 0.02)	
F463	0.85 ± 0.02 (0.85 ± 0.02)	
F464	0.88 ± 0.06 (0.88 ± 0.04)	(47 ± 41)
K465	0.92 ± 0.02 (0.94 ± 0.02)	39 ± 12 (69 ± 60)
R466	0.81 ± 0.04 (0.79 ± 0.05)	
A467	0.96 ± 0.03 (0.93 ± 0.03)	(59 ± 45)
V468	0.86 ± 0.06 (0.81 ± 0.02)	
E469	0.88 ± 0.02 (0.88 ± 0.01)	32 ± 13
G470	0.83 ± 0.04	
Q471		
H472	0.91 ± 0.15	
N473		
Y474	0.85 ± 0.02	
L475		
C476	0.87 ± 0.05	
A477	0.84 ± 0.05	30 ± 27
G478	0.76 ± 0.02	11 ± 11
R479		
N480	0.82 ± 0.03	13 ± 13
D481	0.87 ± 0.05	
C482	0.81 ± 0.03	43 ± 12
I483	0.74 ± 0.02	25 ± 7
I484	≈1 ± 0.05	
D485	0.88 ± 0.04	57 ± 55
K486	0.87 ± 0.05	29 ± 4
I487	0.82 ± 0.07	
R488	0.86 ± 0.02	60 ± 20
R489	≈1 ± 0.05	
K490		
N491		
C492	0.83 ± 0.01	
P493		
A494		
C495	0.80 ± 0.02	29 ± 25
R496	0.98 ± 0.10 (0.93 ± 0.09)	
Y497	0.89 ± 0.01	(0.89 ± 0.01)
R498	0.92 ± 0.03 (0.91 ± 0.03)	
K499	0.84 ± 0.03 (0.86 ± 0.02)	
C500	0.90 ± 0.04 (0.95 ± 0.03)	
L501	0.84 ± 0.07 (0.88 ± 0.05)	
Q502	0.82 ± 0.02 (0.85 ± 0.02)	30 ± 10 (38 ± 20)
A503	0.91 ± 0.02 (0.92 ± 0.02)	
G504	0.81 ± 0.02	17 ± 6
M505	0.82 ± 0.01	24 ± 15
N506	0.91 ± 0.01	≈0 ± 10

[a] Values refer to local optimizations using T_1 and NOE data for each residue, with τ_R = 6.3 ns. Values within parentheses refer to global optimization of local parameters and τ_R using T_1, $T_{1\rho}$, and NOE data for K461–E469 and R496–A503.

20 ps) would exhibit NOEs that are lower than ≈0.78, but larger than ≈0.65, and increased values of T_1 (≈0.5). Flexible loops (with $S^2 < 0.7$) on the protein surface can be expected to exhibit NOEs that are lower than those found in ordered secondary structures and significantly increased T_1 relaxation times. For instance, six consecutive residues in the linker loop joining the two subdomains of calbindin D_{9k} (MW = 8500) showed an average NOE of 0.44 ± 0.13 at a magnetic field of 11.74 T (Kördel et al., 1992). Completely disordered regions of protein fragments can be expected to have even lower and sometimes also negative NOEs. In other studies on ^{15}N-labeled proteins, negative NOEs have been found in terminal segments (Kay et al., 1989; Kördel et al., 1992; Stone et al., 1992).

$T_{1\rho}$ relaxation times are sensitive to picosecond backbone motions as T_1 and the NOE, but also to motions occurring on much longer time scales (milliseconds), due to the $J(\omega_e)$ dependence in eq 3. In this study we only use $T_{1\rho}$ values of hydrogen-bonded amides to characterize the overall rotational motion of the protein.

Backbone Dynamics in the DBD. Inspection of T_1 and NOE data in Figure 4 does not immediately reveal any regions that might be outstanding in terms of extensive backbone flexibility. On the contrary, our data suggest that rapid motions are largely restricted and uniform throughout the GR DBD backbone. In particular, the relative flexibility of the two zinc binding domains does not seem to be significantly different from that of the helical domains. A closer inspection reveals a limited number of short sequences that perhaps might be more flexible, although it should be kept in mind that deviations from average T_1 and NOE values discussed below are very small. For instance, the short segment S448–H451, located in a surface loop in the first zinc domain (Figure 1), might be somewhat more flexible than the remainder of the protein, since residues S448 and G449 both show NOE values that are significantly lower than the average (0.68 and 0.62, respectively). Unfortunately, there are no reliable T_1 data for these residues and no T_1 or NOE data for residues C450 or H451, because of missing ^{15}N resonance assignments. A definite conclusion regarding the flexibility of the S448–H451 loop is therefore not possible. Similarly, the NOE of E508 is low (0.58), suggesting that the amide of this residue is more mobile. E508 is the most C-terminal residue for which an NOE could be measured. The residues R510–Q520 are disordered in both the X-ray and NMR structures of the DBD, and only a few weak sequential NOEs can be detected for E508 and A509 in NOESY spectra, suggesting a poor definition of the backbone also for these two residues (Härd et al., 1990b). Thus, it is possible that the high flexibility and disorder of the C-terminal part of the DBD fragment begins around E508.

Residues Y474–L475, located within an extended region where some of the other amide protons are subjected to solvent exchange, also have low NOEs, albeit with somewhat large uncertainties. The T_1 relaxation rate of Y474, on the other hand, is very similar to those measured within the helices. The N-terminal end of the β strand within the second zinc domain (D481–I483) might also be somewhat more flexible, as judged from three consequtive NOEs which are all less than 0.7, and a long T_1 relaxation time (0.54 ± 0.02) for the amide ^{15}N of I483. NOEs and T_1 relaxation times for four of the six residues in the C-terminal part of the second zinc domain do not suggest a disordered or flexible structure. This is the region where a helix is found in the crystal structure but not in the NMR structure, as discussed in the introductory section. Unfortunately, no reliable data are available for the residues K490 and N491 within this region, and no conclusions can be drawn for these two residues.

Table III: Average S^2 Order Parameters for DBD

domain	residues	residues for which S^2 is determined	average S^2
helix I	C457–E469	C457–C469	0.89 ± 0.05
helix II	K486–N491	K486–R489	0.89 ± 0.08
helix III	C492–A503	C492, C496–A503	0.87 ● 0.06
1st zinc domain	C440–C460	C440–A447, G453–C457, S459–C460	0.88 ● 0.06
2nd zinc domain	C476–C495	C476–G478, N480–R489, C492, C495	0.85 ± 0.7

A quantitative evaluation of the model parameters for internal motions requires considerable caution to avoid overinterpretation of experimental data. It is tempting to embark on detailed analyses applying various models for internal motions and slower motions (affecting $T_{1\rho}$), using statistical methods to discriminate between various possibilities. In this study, however, we have chosen to use only the NOE and T_1 data in combination with the spectral density function of eq 4. The parameters characterizing internal motions, S^2 and τ_e, were calculated for 53 (of 66) residues within the C440–N506 using Monte Carlo simulations of experimental data to estimate uncertainties, as described in the Materials and Methods section. All results presented here were calculated using the optimized value of τ_R = 6.3 ns, but calculations carried out using other lower τ_R values (not shown) yield similar results and would not conflict with any conclusions regarding DBD backbone dynamics.

Optimized values for the S^2 order parameters are given in Table II and are also shown in Figure 4. A quantitative evaluation is lacking for some regions due to insufficient T_1 data. For instance, the dynamics within the loop region S448–Y452 within the first zinc domain could not be quantitatively evaluated. Accuracies in determined values are rather high for 37 (of 53) S^2 determinations ($\sigma_{S^2} \leq 0.05$), fair for 15 determinations ($0.05 < \sigma_{S^2} \leq 0.10$), and poor for 1 residue (H472), for which $\sigma_{S^2} = 0.15$. The effective correlation time τ_e is more sensitive to uncertainties in experimental data, and this parameter could only be determined for 18 residues. The determined τ_e correlation times are all less than 100 ps, with an average of 36 ± 26 ps.

The quantitative evaluation of internal backbone motions in DBD agrees well with the qualitative indications discussed above. The average flexibility is very similar in the various structural domains, as shown in Table III. Average optimized S^2 parameters for various regions of the GR DBD (Table III) fall within the same ranges (approximately =0.88 ± 0.07) found in stable regions of other proteins. Average S^2 values obtained for the two well-defined α-helices C457–E469 and C492–A503 (0.89 ± 0.05 and 0.89 ± 0.09, respectively) are also very similar to the order parameters of α-helical domains in other studies (Kay et al., 1989; Clore et al., 1990a; Kördel et al., 1992). Only two residues, G478 and I483, exhibit S^2 order parameters which are significantly lower than the average ($S^2 = 0.76 \pm 0.02$ and $S^2 = 0.74 \pm 0.02$, respectively). The unassigned amide nitrogen, which might belong to Q520, has optimized values of $S^2 = 0.11 \pm 0.015$ and $\tau_e = 214 \pm 12$ ps.

Calculated S^2 values for four of six residues within the region of the second finger domain that is helical in the DBD–DNA complex, as discussed above, are all within a range corresponding to an ordered moderately flexible backbone conformation. These data therefore suggest that the apparent

disorder observed in the NMR structure (Härd et al., 1990b) is due to a lack of structural constraints. One might reflect that the present method of monitoring backbone flexibility and disorder for some reasons is insensitive to motions in disordered regions and that relaxation and NOE data cannot be used to identify disordered regions. However, there is a large body of evidence from other studies contradicting such a suggestion. For instance, the NMR structure determination of the "linker loop" in calbindin D_{9k} yielded disordered conformations whereas the precision obtained for other parts of the protein was high (Kördel, 1991). In this case, however, the average order parameters for four residues in the loop region ($S^2 \approx 0.4$) was significantly lower than in ordered regions (Kördel et al., 1992), indicating that the disorder observed in the structure calculations indeed reflects larger flexibility.

Structural and Functional Implications of DBD Backbone Dynamics. In this paper we show that the internal flexibility of the peptide backbone in the GR DBD at 299 K, pH 7.6, is uniform and limited on short time scales ($\leq$1 ns). Our results suggest that no part of the DBD is highly flexible in solution, with the possible exception of residues S448–H451 of the first zinc domain and a few other very short peptide segments for which relaxation parameters could not be obtained. The amides of some residues, including G478, I483, and E508, seem somewhat more mobile than the average.

Our results do not, on the other hand, exclude the possibility of slower exchange processes between conformational substates. Exchange that occurs on time scales coinciding with the field strength of the spin lock field used in the $T_{1\rho}$ experiment might affect the $T_{1\rho}$ relaxation times of the involved nuclei through $J(\omega_e)$ in eq 3. In this study we only use $T_{1\rho}$ relaxation times of residues that are involved in hydrogen bonding in α-helices, for which millisecond exchange processes are unlikely. A quantitative evaluation of slow exchange processes should probably also include T_2 measurements using CPMG delays of varying lengths in combination with pulse sequences or data analysis that account for the evolution of antiphase coherences.

Our results are somewhat unexpected considering recent findings and discussions concerning the structure of the second zinc domain in the free and complexed state. The discussion has concerned the fact that the second zinc domain appears to be largely disordered in NMR structure determinations of the DNA-binding domains of GR (Härd et al., 1990b) and ER (Schwabe et al., 1990), whereas it is ordered in the crystal structure of a GR DBD–DNA complex (Luisi et al., 1991). It has been suggested that binding to DNA stabilizes the second zinc domain through interactions with DNA and through protein–protein interactions in the bound dimer (Luisi et al., 1991). However, our results indicate that the second zinc domain in fact is well-ordered in the uncomplexed state and that there is some other reason for the poor definition of this domain in the NMR structure determinations.

The accuracy of NMR structure determinations is dependent on the number of NOE connectivities and J couplings used as structural constraints. Of particular importance are long-range NOE connectivities, i.e., NOEs between residues far apart in the sequence. Inspection of the crystal structure shows that there is only a small number of crucial interresidue ^{1}H–^{1}H distances within the second zinc domain, which would enforce a well-defined structure in distance geometry and/or simulated annealing. If some of the corresponding ^{1}H resonances are overlapped (which they are), then it is "inherently" difficult to determine the structure of this domain with NMR.

In this context it is important to note that the present studies have been carried out at pH 7.6, whereas previous NMR structure determinations of the GR and ER DBDs were carried out using data collected at pH values around 6.5 (Härd et al., 1990b; Schwabe et al., 1990). Backbone flexibility might depend on the pH if zinc ion exchange rates increase as the pH is lowered and approaches a value at which the zinc ions no longer are strongly coordinated in the protein. The issue of pH-dependent zinc coordination and exchange rates has, to our knowledge, not yet been investigated in detail, but the critical pH is certainly higher than 4.5 (K. Dahlman-Wright, unpublished results). Thus, it is conceivable that the conformational flexibility within the second zinc domain is larger at pH 6.5 due to a more rapid zinc ion exchange and that this effect attenuates medium- and long-range NOEs, thereby diminishing the number of observable NOEs and explaining the poor resolution of this domain in previous NMR structure determinations. On the other hand, one might expect such a mechanism to be accompanied by an increased line broadening of ^{1}H resonances in residues involved in the exchange processes. We have not noticed any significant sharpening of ^{1}H resonances in our samples of DBD-82 at pH 7.6 compared to previous spectra of similar protein fragments at lower pH values (Härd et al., 1990a). Still, possible effects due to zinc ion exchange cannot be ruled out, and this issue is presently being investigated in more detail in our laboratory.

Our results indicate that there is a well-defined backbone conformation in DBD at pH 7.5. However, the present results do not exclude the possibility of a conformational change (from one ordered state to another) within the second zinc domain upon binding to DNA. This issue can only be resolved by comparing a well-refined structure of DBD in solution to that of the present crystal structure of the DBD–DNA complex (Luisi et al., 1991) and/or observing significant differences between the NMR spectra of DBD in the free and DNA-complexed states in solution.

ADDED IN PROOF

The predicted error in the published sequence of the yeast OSM1 gene has now been confirmed experimentally (L. Melnick, personal communication). The OSM1 protein sequence shown in Figure 4 is therefore confirmed to be correct.

ACKNOWLEDGMENT

We thank Prof. Paul Sigler for providing crystal coordinates of the DBD–DNA complex and Dr. Per Kraulis for providing the MolScript program used to prepare Figure 1. Dr. Tony Wright at the Center for Biotechnology, Karolinska Institute, is acknowledged for assistance in protein purification. Dr. Johan Kördel is acknowledged for useful advice concerning the recording and interpretation of NMR relaxation data.

REFERENCES

Abragam, A. (1961) in *The Principles of Nuclear Magnetism*, Clarendon Press, Oxford.

Bax, A., Griffey, R. H., & Hawkins (1983) *J. Am. Chem. Soc. 105*, 7188–7190.

Bax, A., Sparks, S. W., & Torchia, D. A. (1989) *Methods Enzymol. 176*, 134–150.

Bax, A., Ikura, M., Kay, L. E., Torchia, D. A., & Tschudin, R. (1990) *J. Magn. Reson. 86*, 304–318.

Bodenhausen, G., & Ruben, D. J. (1980) *Chem. Phys. Lett. 69*, 185–189.
Cantor, R. C., & Schimmel, P. R. (1980) in *Biophysical Chemistry*, W. H. Freeman, San Francisco.
Clore, G. M., Driscoll, P. A., Wingfield, P. T., & Gronenborn, A. M. (1990a) *Biochemistry 29*, 7387–7401.
Clore, G. M., Szabo, A., Bax, A., Kay, L. E., Driscoll, P. A., & Gronenborn, A. M. (1990b) *J. Am. Chem. Soc. 112*, 4989–4991.
Dahlman, K., Strömstedt, P.-E., Rae, C., Jörnvall, H., Flock, J.-I., Carlstedt-Duke, J., & Gustafsson, J.-A. (1989) *J. Biol. Chem. 264*, 804–809.
Danielsen, M., Hinck, L., & Ringold, G. (1989) *Cell 57*, 1131–1138.
Evans, R. M. (1988) *Science 240*, 889–895.
Freedman, L. P., Luisi, B. F., Korzun, Z. R., Basavappa, R., Sigler, P. B., & Yamamoto, K. R. (1988) *Nature 334*, 543–546.
Griesinger, C., Otting, G., Wüthrich, K., & Ernst, R. R. (1988) *J. Am. Chem. Soc. 110*, 7870–7872.
Gronenborn, A. M., Bax, A., Wingfield, P. T., & Clore, G. M. (1989a) *FEBS Lett. 243*, 93–98.
Gronenborn, A. M., Wingfield, P. T., & Clore, G. M. (1989b) *Biochemistry 28*, 5081–5089.
Härd, T., Kellenbach, E., Boelens, R., Kaptein, R., Dahlman, K., Carlstedt-Duke, J., Freedman, L. P., Maler, B. A., Hyde, E. I., Gustafsson, J.-A., & Yamamoto, K. R. (1990a) *Biochemistry 29*, 9015–9023.
Härd, T., Kellenbach, E., Boelens, R., Maler, B. A., Dahlman, K., Freedman, L. P., Carlstedt-Duke, J., Yamamoto, K. R., Gustafsson, J.-A., & Kaptein, R. (1990b) *Science 249*, 157–160.
Härd, T., Dahlman, K., Carlstedt-Duke, J., Gustafsson, J.-Å., & Rigler, R. (1990c) *Biochemistry 29*, 5358–5364.
Hiyama, Y., Niu, C., Silverton, J. V., Bavoso, A., & Torchia, D. A. (1988) *J. Am. Chem. Soc. 110*, 2378.
Kaptein, R. (1991) *Curr. Opin. Struct. Biol. 1*, 63–70.
Kay, L. E., Torchia, D. A., & Bax, A. (1989) *Biochemistry 28*, 8972–8979.
Keiter, E. A. (1986) Ph.D. Thesis, University of Illinois.
Kördel, J. (1991) Structure and Dynamics of Calbindin D_{9k} as Studied by 2D NMR, Ph.D. Thesis, University of Lund.
Kördel, J., Skelton, N. J., Akke, M., Palmer, A. G., & Chazin, W. J. (1992) *Biochemistry 31*, 4856–4866.
Levy, G. C., & Lichter, R. L. (1979) in *Nitrogen-15 Nuclear Magnetic Resonance Spectroscopy*, p 59, John Wiley, New York.
Lipari, G., & Szabo, A. (1982a) *J. Am. Chem. Soc. 104*, 4546–4559.
Lipari, G., & Szabo, A. (1982b) *J. Am. Chem. Soc. 104*, 4559–4570.
Luisi, B. F., Xu, W. X., Otwinowski, Z., Freedman, L. P., Yamamoto, K. R., & Sigler, P. B. (1991) *Nature 352*, 497–505.
Mader, S., Kumar, V., de Verneuil, H., & Chambon, P. (1989) *Nature 338*, 271–274.
Marion, D., & Wüthrich, K. (1983) *Biochem. Biophys. Res. Commun. 113*, 967–974.
Marion, D., Driscoll, P. C., Kay, L. E., Wingfield, P. T., Bax, A., Gronenborn, A. M., & Clore, G. M. (1989a) *Biochemistry 28*, 6150–6156.
Marion, D., Ikura, M., & Bax, A. (1989b) *J. Magn. Reson. 84*, 425–430.
McCammon, J. A., & Harvey, S. C. (1987) in *Dynamics of Proteins and Nucleic Acids*, Cambridge University Press, Cambridge, England.
Müller, L. (1979) *J. Am. Chem. Soc. 101*, 4481–4484.
Nirmala, N. R., & Wagner, G. (1988) *J. Am. Chem. Soc. 110*, 7557–7558.
Palmer, A. G., Rance, M., & Wright, P. E. (1991) *J. Am. Chem. Soc. 113*, 4371–4380.
Peng, J. W., Thanabal, V., & Wagner, G. (1991a) *J. Magn. Reson. 94*, 82–100.
Peng, J. W., Thanabal, V., & Wagner, G. (1991b) *J. Magn. Reson. 95*, 421–427.
Press, W. H., Flannery, B. P., Teukolsky, S. A., Vetterling, W. T. (1986) in *Numerical Recipes*, Chapter 14, Cambridge University Press, Cambridge, England.
Schena, M., Freedman, L. P., & Yamamoto, K. (1989) *Genes Dev. 3*, 1590–1601.
Schneider, D. M., Dellwo, M. J., & Wang, A. J. (1992) *Biochemistry 31*, 3645–3652.
Schwabe, J. W. R., Neuhaus, D., & Rhodes, D. (1990) *Nature 348*, 458–461.
Smith, G. P., Yu, L. P., & Domingues, D. J. (1987) *Biochemistry 26*, 2202–2207.
States, D. J., Haberkorn, R. A., & Ruben, D. J. (1982) *J. Magn. Reson. 48*, 286–292.
Stone, M. J., Fairbrother, W. J., Palmer, A. G., Reizer, J., Saier, M. H., & Wright, P. E. (1992) *Biochemistry 31*, 4394–4406.
Tabor, S., & Richardson, C. C. (1985) *Proc. Natl. Acad. Sci. U.S.A. 82*, 1074–1078.
Umesuno, K., & Evans, R. M. (1989) *Cell 57*, 1139–1146.
Wüthrich, K., & Wagner, G. (1979) *J. Mol. Biol. 130*, 1–18.